ADVANCED MATERIALS

Supporting Information

for *Adv. Mater.*, DOI: 10.1002/adma.201803165

A Real-Time Wearable UV-Radiation Monitor based on a High-Performance p-CuZnS/n-TiO_2 Photodetector

Xiaojie Xu, Jiaxin Chen, Sa Cai, Zhenghao Long, Yong Zhang, Longxing Su, Sisi He, Chengqiang Tang, Peng Liu, Huisheng Peng, and Xiaosheng Fang**

ADVANCED MATERIALS

Supporting Information

for *Adv. Mater.*, DOI: 10.1002/adma.201803165

Real-time Wearable UV Radiation Monitor based on High-performance p-CuZnS/n-TiO_2 Photodetector

Xiaojie Xu, Jiaxin Chen, Sa Cai, Zhenghao Long, Yong Zhang, Longxing Su, Sisi He, Chengqiang Tang, Peng Liu, Huisheng Peng and Xiaosheng Fang**

Dr. X. J. Xu, J. Chen, S. Cai, Z. Long, Dr. Y. Zhang, Dr. L. Su and Prof. X. S. Fang

Department of Materials Science

Fudan University, Shanghai 200438, China.

Dr. X. J. Xu, Dr. S. He, C. Tang, Dr. P. Liu and Prof. H. S. Peng

State Key Laboratory of Molecular Engineering of Polymers

Department of Macromolecular Science, and Laboratory of Advanced Materials

Fudan University, Shanghai 200438, China.

Email: penghs@fudan.edu.cn; xshfang@fudan.edu.cn

XRD and WAXS analysis

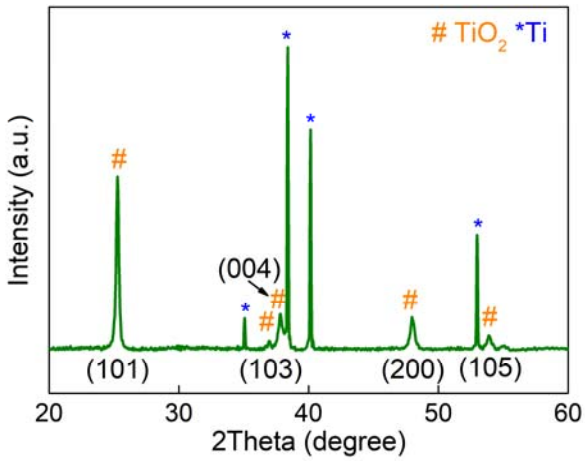

Figure S1. The XRD of TiO_2 nanotube arrays.

In Figure S1, the sharp peak located at ~25.3° is assigned to (101) facet of anatase TiO_2 (JCPDS card no. 21-1272), while other strong peaks match well with Ti substrate (JCPDS no.1-1197).[1]

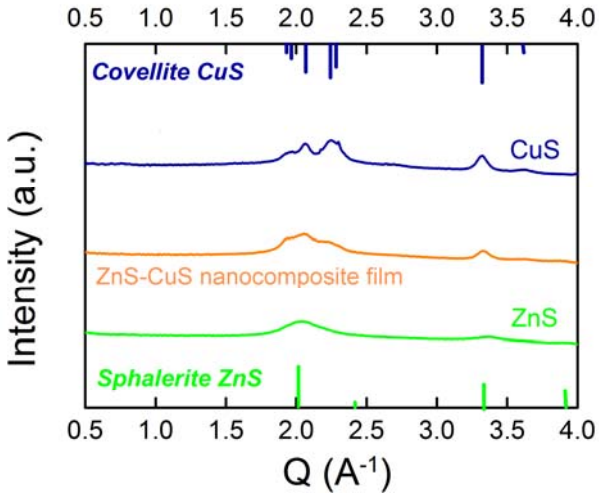

Figure S2. The WAXS pattern of CuS-ZnS nanocomposite film.

As the nanocrystals in CuZnS film are too small to be detected via commercial XRD measurement, wide-angle X-ray scattering (WAXS) was used to identify the crystalline phases in CuZnS, where the mixed crystalline phases of sphalerite ZnS and covellite CuS are present in the CuS-ZnS nanocomposite film.

Morphology, composition and crystallinity study of the conformal CuZnS coating on TiO_2 nanotube arrays (NTAs)

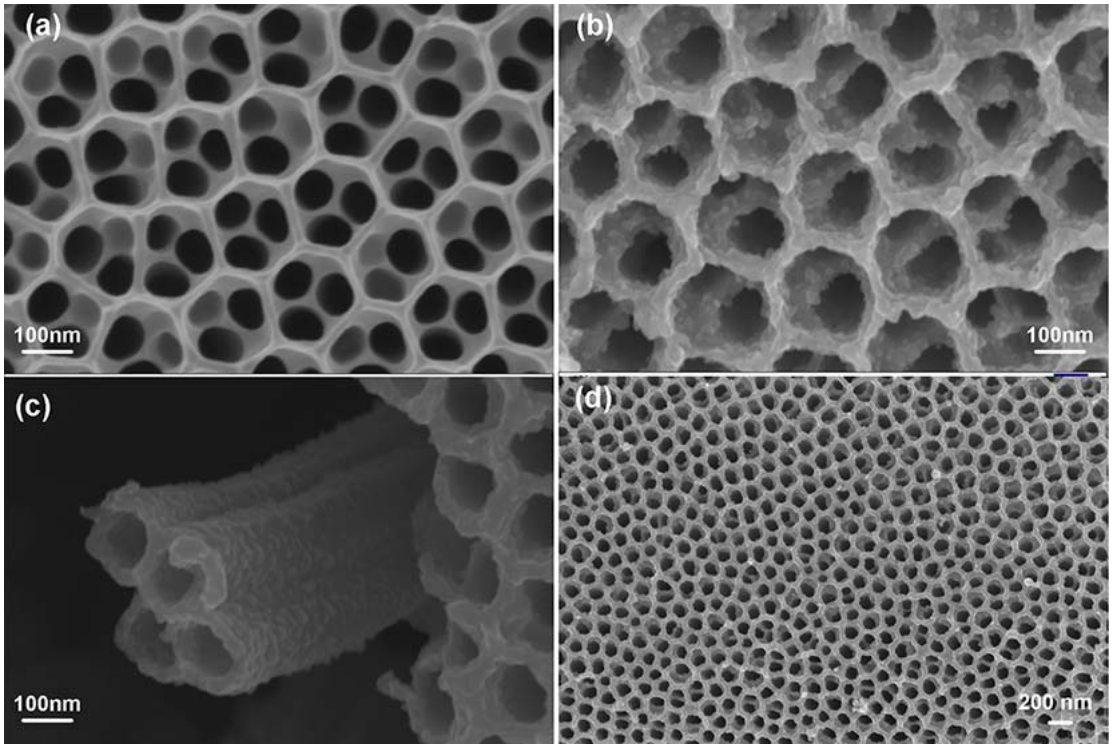

Figure S3. The SEM images of TiO_2 NTAs with and without CuZnS coating layer. (a) Pristine TiO_2 NTAs; (b) Conformal coating of CuZnS on TiO_2 NTAs; (c) Side view of separated TiO_2 nanotubes coated with CuZnS; (d) Zoomed-out SEM image of TiO_2 NTAs with CuZnS.

The SEM images at different scales and angles indicate the conformal coating of CuZnS on TiO_2 NTAs.

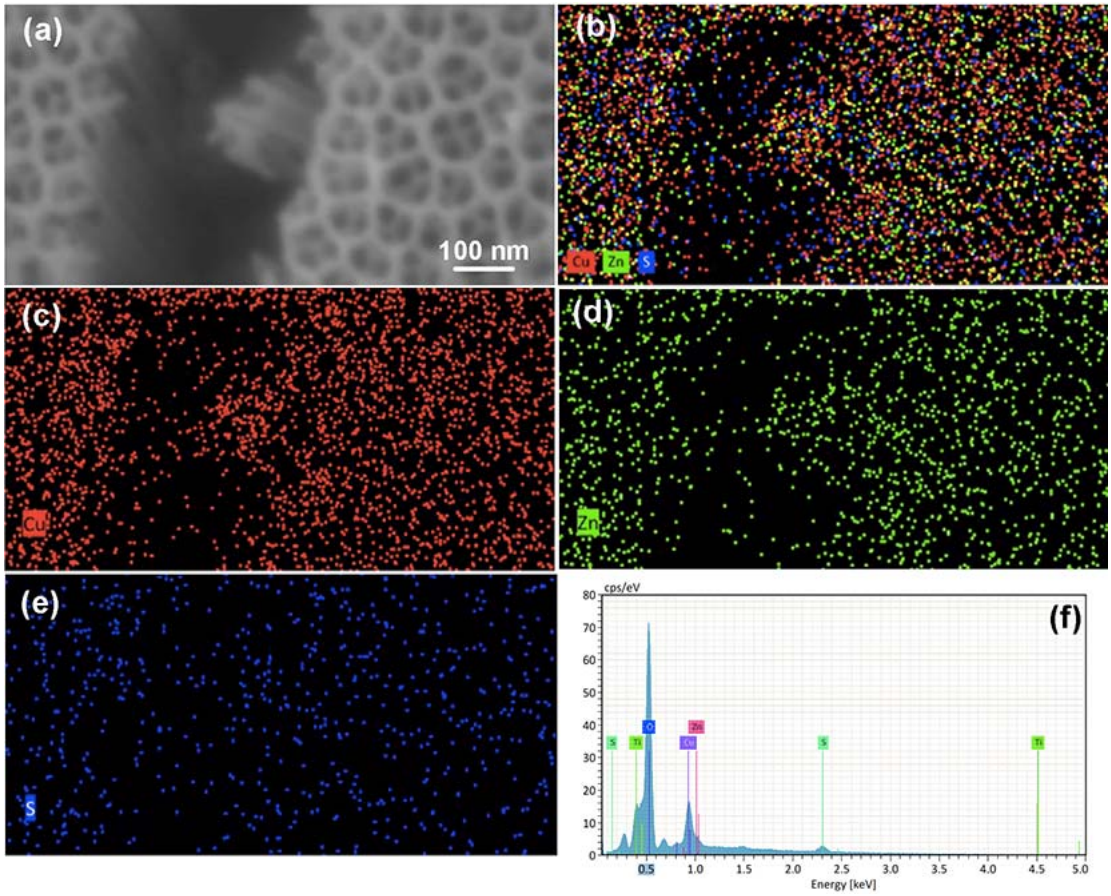

Figure S4. The EDS study of CuZnS layer on TiO_2 NTAs. (b) - (e) depict the uniform distribution of elements: Cu, Zn and S in the CuZnS layer on (a) TiO_2 NTAs, respectively. (f) EDS spectra of CuZnS/TiO_2 NTAs.

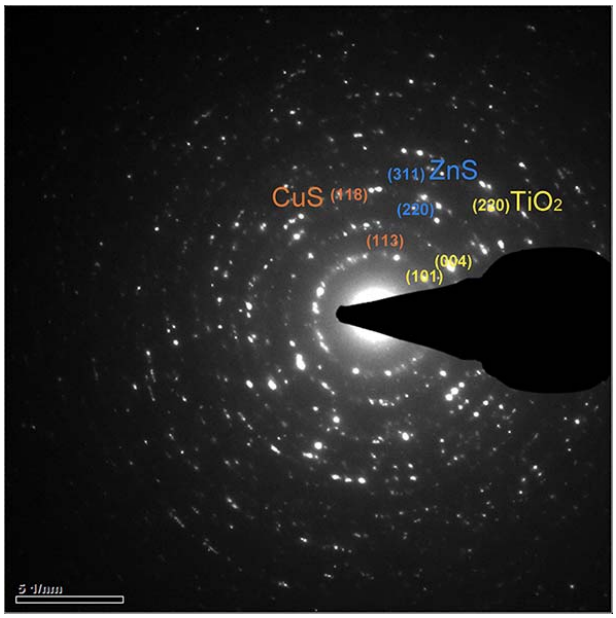

Figure S5. The SAED pattern of p-CuZnS/n-TiO_2 NTAs.

The corresponding SAED pattern of CuZnS on TiO_2 NTAs shows the mixed phases of ZnS and CuS, indicating the successful deposition of CuS-ZnS nanocomposite film on TiO_2 NTAs. It agrees well with the HRTEM image in Figure 2d.

Optical properties of CuZnS and TiO_2 NTAs

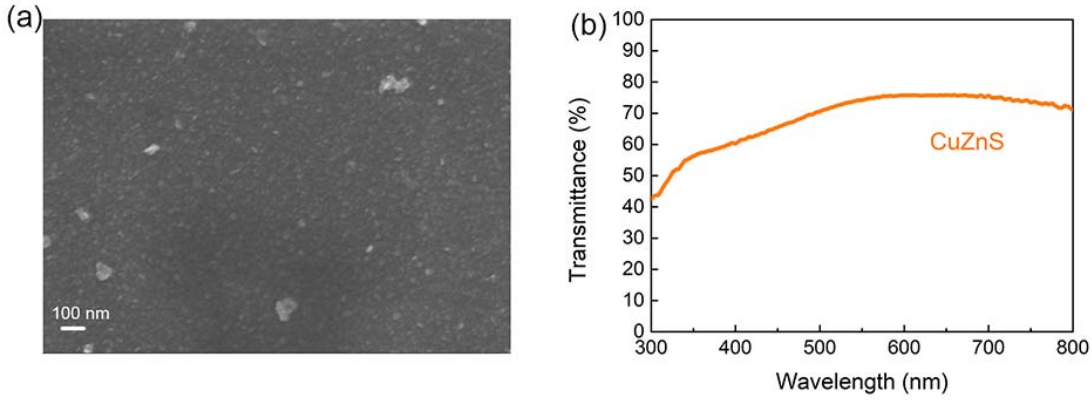

Figure S6. (a) SEM image of CuZnS film on Si substrates and (b) transmittance spectra of CuZnS on quartz substrates.

The morphology of the CuZnS film deposited on Si substrates is identical to the one grown on TiO_2 NTAs. It shows an average transmittance of ~75% in the visible range, which agrees well with our previous reports.

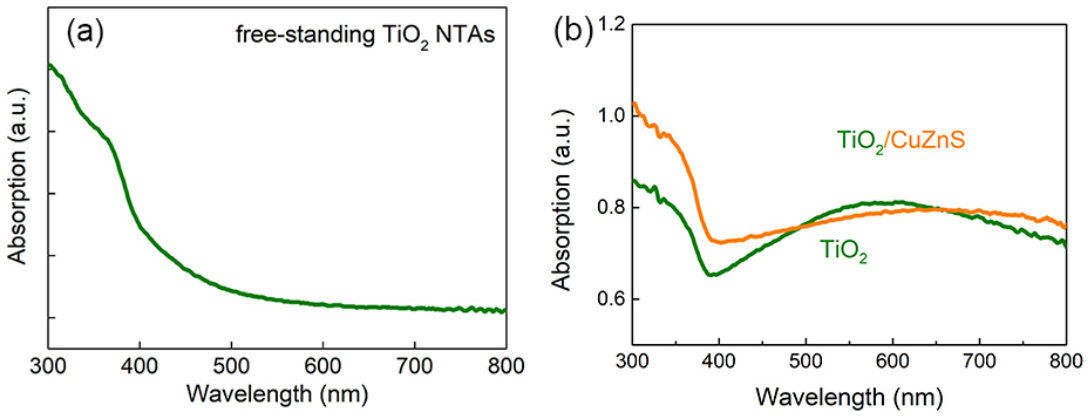

Figure S7. UV-vis absorption spectra of (a) free-standing TiO_2 NTAs peeled off from Ti metal substrates and (b) TiO_2 NTAs and CuZnS/TiO_2 on Ti foils.

Figure S7b suggests that TiO_2 nanotube arrays have a strong absorption towards UV region. Compared with the absorption of free-standing TiO_2 NTAs in Figure S7a, the wide absorption towards visible region of planar TiO_2 NTAs may come from the absorption of Ti foils. With the coating of CuZnS, the UV absorption is greatly enhanced while the absorption spectra in the visible range remains almost unchanged, further suggesting the conformal and uniform coating of transparent CuZnS layer on TiO_2 NTAs.

Optoelectronic performance of planar PDs

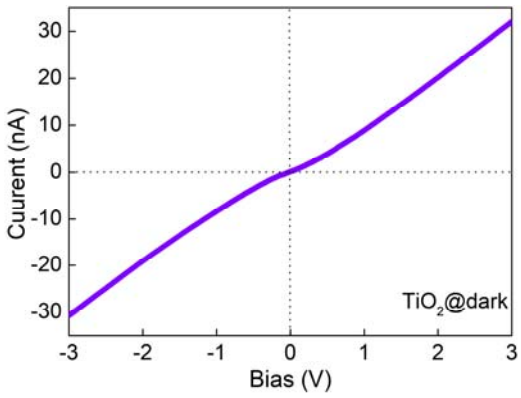

Figure S8. The linear current–voltage curve of TiO_2 NTAs on Ti foils in dark.

The close-to-linear *I-V* curve in dark conditions shown in Figure S8 indicates that the Schottky barrier between Ag elecrtrodes and TiO_2 is insufficient to produce a self-powered photocurrent.

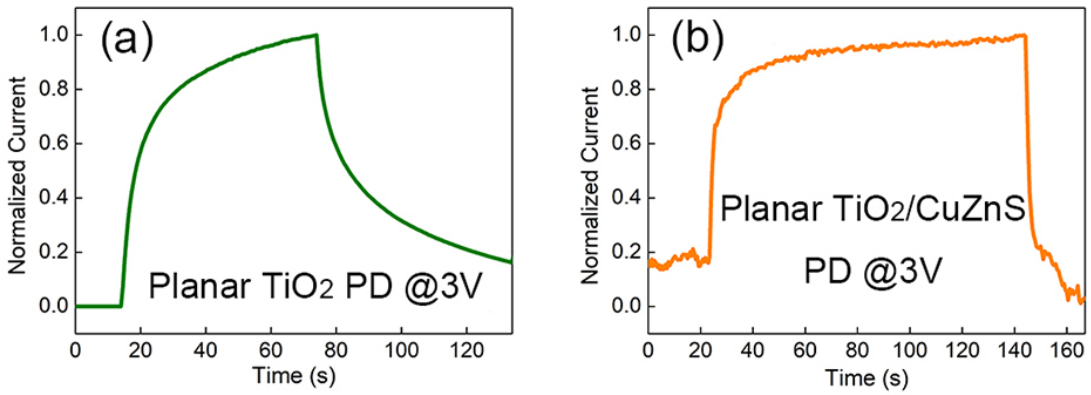

Figure S9. The time domain photoresponse curve of (a) pure TiO_2 NTAs grown on Ti foils under 350 nm illumination at 3 V bias and (b) p-CuZnS/n-TiO_2 on Ti foils under 350 nm illumination at 3 V.

The *I-t* curves in Figure S9 indicate that the response time of the planar p-CuZnS/n-TiO_2 PD is dramatically decreased compared with that of the pure TiO_2 NTAs PD under the same test conditions.

Effect of anodization time on the properties of fiber-shaped PDs

To gain more insight into how the material properties affect the device performance, we adjusted the length and morphology of the TiO_2 NTAs grown on Ti wire by prolonging the anodization time from 10 minutes to 2 hours. Herein, we further explored the morphologies and optoelectronic performance of those devices, named 10min-TiO_2 NTAs and 2h-TiO_2 NTAs, respectively.

Morphology of TiO_2 NTAs grown on Ti wire under different conditions

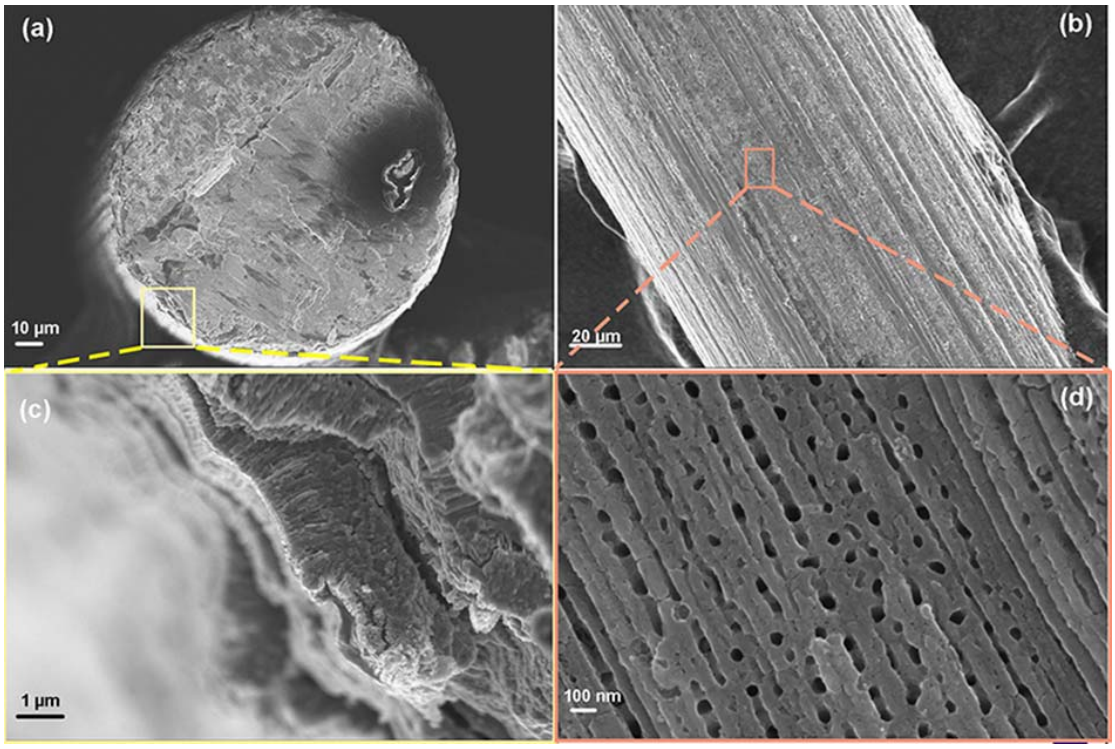

Figure S10. SEM images of (a) cross-section and (b) top view of 10min-TiO_2 NTAs formed on Ti wires. (c) and (d) are the magnified images of framed parts in (a) and (b), respectively.

As can be seen from Figure S10, it should be pointed out that TiO_2 nanotubes are grown radially and uniformly around the Ti wire core.

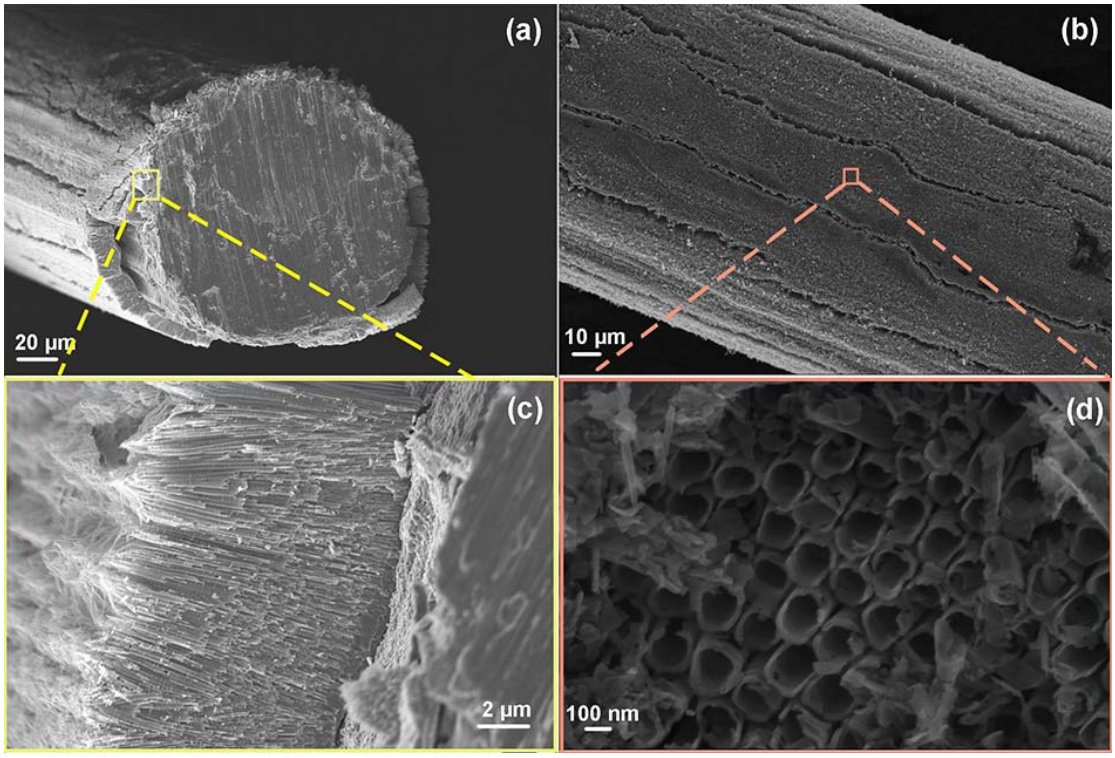

Figure S11. SEM images of (a) cross-section and (b) top view of 2h-TiO_2 NTAs. (c) and (d) are the magnified image of framed parts in (a) and (b), respectively.

Compared with Figure S10, after two-hour anodization, the length of TiO_2 nanotubes is greatly enhanced and they are still uniformly and closely aligned on the surface of Ti wire. Figure S11d suggests a longer anodization process is likely to promote the formation of a better nanotube structure.

Figure S12. Digital photograph of the fiber-shaped UV sensor.

Figure S12 shows a typical photograph of a fiber-shaped CuZnS/TiO_2 PD.

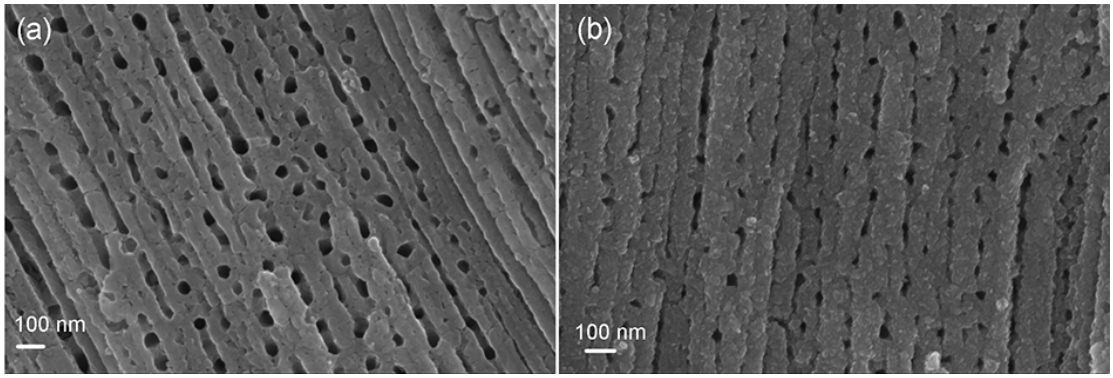

Figure S13. SEM images of TNAs (a) before and (b) after confomal coating of CuZnS on 10min-TiO_2 NTAs.

Figure S13 further demonstrates the conformal coating of CuZnS on the TiO_2 TNAs grown on Ti wire.

Ultraviolet photoelectron spectroscopy

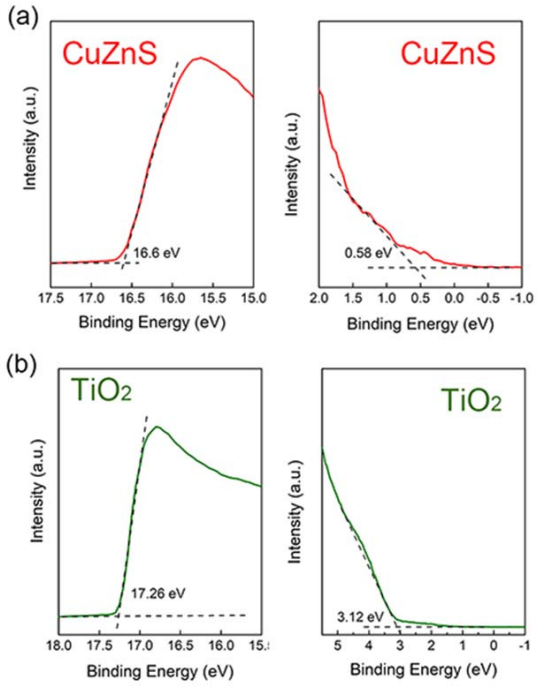

Figure S14. Ultraviolet photoelectron spectroscopy (UPS) results of (a) CuZnS and (b) TiO_2 NTAs .

Ultraviolet photoelectron spectroscopy (UPS) was carried out to study the electronic structure of p-CuZnS and n-TiO_2.

Optoelectronic performance of other fiber-shaped CuZnS/TiO_2 PDs

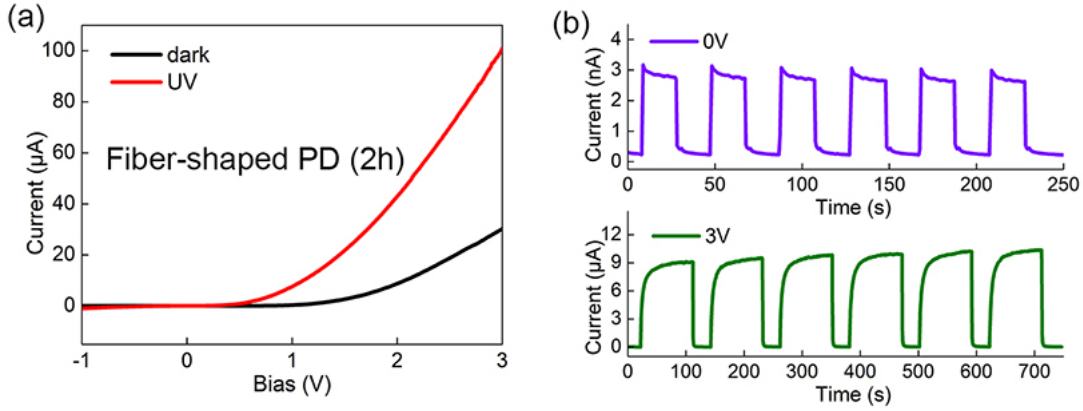

Figure S15. The optoelectronic measurements of CuZnS/2h-TiO_2 NTAs PD. (a) *I-V* characteristic of fiber-shaped CuZnS/TiO_2 PD in dark and under UV illumination. (b) Time dependence of photocurrent for fiber-shaped CuZnS/TiO_2 PD at 0 V and 3 V bias.

Figure S15 manifests that 2h-PDs also possess a significant rectification effect and quite stable on-off properties, which is consistent with that of the 10min-PD. Note that the response speed and photocurrent of 2h-PDs show a slight decrease relative to 10min-PDs. The rise and decay time of 2h-PDs are 0.8 s/0.7 s at 0 V bias and 19.2 s/1.5 s at 3 V bias. Considering the superior performances of 10min-PDs, 10min-TiO_2 NTAs were chosen for further study and application.

Bending tests

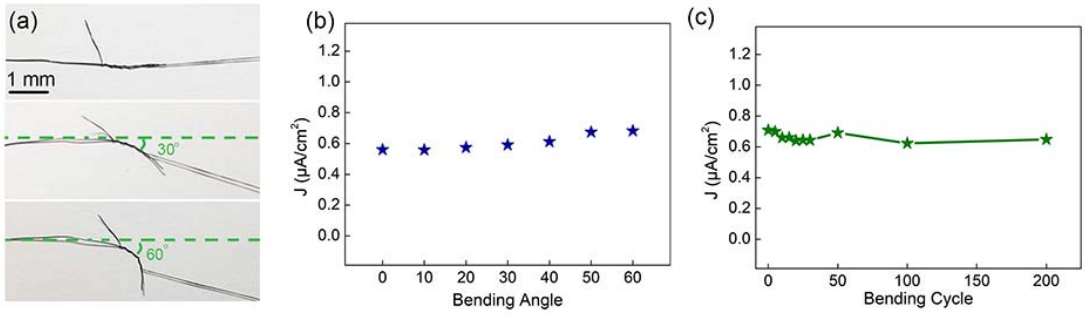

Figure S16. Bending tests of fiber-shaped PDs. (a) Photographs of the fiber-shaped PD operated under different bending conditions. (b) Photocurrent density of fiber-shaped PD under different bending angles. (c) Photocurrent tests of fiber-shaped PD after a few hundred bending cycles under 60°.

The systematic bending tests further verify the wearable properties of fiber-shaped PDs. As shown in Figure S16b and S16c, the photocurrent density almost remains unchanged under a series of bending angles and after given bending cycles, which implies that the device owns a presentable stability and durability.

Table S1. Electronic properties of CuZnS and TiO_2 nanotube arrays.

Materials	**Resistivity (Ω cm)**	**Carrier concentration (cm^{-3})**	**Mobility ($cm^2/(Vs)$)**	**Carrier type**	**Ref.**
CuZnS	2.1×10^{-3}	2.0×10^{21}	1.5	P	-
TiO_2	10.2	1.7×10^{17}	3.6	N	[2]

Table S2. Comparison of the main parameters for CuZnS/TiO_2 PDs and other PDs in literature.

Materials	Wavelength/nm	Bias/V	Photocurrent	Responsivity/ A W^{-1}	EQE/%	Rise time	Decay time	Wearable	Ref.
BiOCl/TiO_2	350	-5	0.783 mA	41.94	-	12.9 s	0.81 s	No	[3]
TiO_2/ZnO/SiO_2	370	1	182 μA	-	-	-	-	No	[4]
Si/TiO_2	400 400	0 -4	- -	~10-6 >10-1	- -	- -	- -	No	[5]
$MAPbI_3$/TiO_2	350	1	44 nA	1.3	-	2 s	1 s	No	[6]
Se/TiO_2	350 350	0 1	18.3 nA -	- -	- -	- 67.4 s	- 76.7 s	No	[1]
PBDTT-DPP: $PC_{71}BM$	735	1	-	29.69	5008.9	162 μs (780	7.9 ms (780	No	[7]

						nm)	nm)		
$MAPbI_3/TiO_2$	**550**	**-0.7**	**-**	**620**	**2.4×10^5**	**-**	**-**	**No**	**[8]**
P3HT:PCBM:Ir-125:Q-switch 1	**510**	**-3.7**	**-**	**23.0**	**5500**	**-**	**-**	**No**	**[9]**
C-TPD:ZnO	**390**	**-8**	**-**	**1.28**	**408**	**-**	**-**	**No**	**[10]**
P3HT:ZnO	**360**	**-9**	**-**	**1001**	**3.4×10^5**	**25 µs**	**558 µs**	**No**	**[11]**
$CuZnS/TiO_2$	**300**	**0**	**~28 nA**	**2.54×10^{-3}**	**1.0**	**<0.2 s**	**<0.2 s**	**Yes**	**This work**
(fiber-shaped)	**350**	**3**	**~4 mA**	**640**	**2.3×10^5**	**14.4 s**	**8.5 s**		

References

[S1] L. Zheng, K. Hu, F. Teng, X. S. Fang, *Small* **2017**, *13*, 1602448.

[S2] M. Hattori, K. Noda, T. Nishi, K. Kobayashi, H. Yamada, K. Matsushige, *Appl. Phys. Lett.* **2013**, *102*, 43105.

[S3] W. Ouyang, F. Teng, X. S. Fang, *Adv. Funct. Mater.* **2018**, *28*, 1707178.

[S4] N. Nasiri, R. Bo, T. F. Hung, V. A. L. Roy, L. Fu, A. Tricoli, *Adv. Funct. Mater.* **2016**, *26*, 7359.

[S5] T. Ji, Q. Liu, R. Zou, Y. Sun, K. Xu, L. Sang, M. Liao, Y. Koide, L. Yu, J. Hu, *Adv. Funct. Mater.* **2016**, *26*, 1400.

[S6] Z. Zheng, F. Zhuge, Y. Wang, J. Zhang, L. Gan, X. Zhou, H. Li, T. Zhai, *Adv. Funct. Mater.* **2017**, *27*, 1703115.

[S7] R. Nie, X. Deng, L. Feng, G. Hu, Y. Wang, G. Yu, J. Xu, *Small* 2017, 13, 1603260.

[S8] H. W. Chen, N. Sakai, A. K. Jena, Y. Sanehira, M. Ikegami, K. C. Ho, T. Miyasaka, *J. Phys. Chem. Lett.* 2015, 6, 1773.

[S9] S. T. Chuang, S. C. Chien, F. C. Chen, *Appl. Phys. Lett.* 2012, 100, 13309.

[S10] Y. Fang, F. Guo, Z. Xiao, J. Huang, *Adv. Opt. Mater.* 2014, 2, 348.

[S11] F. Guo, B. Yang, Y. Yuan, Z. Xiao, Q. Dong, Y. Bi, J. Huang, *Nat. Nanotechnol.* 2012, 7, 798.